

Higher moments of the velocity distribution function in dense-gas shocks

Journal Article**Author(s):**

Schlamp, Stefan; Hathorn, Bryan C.

Publication date:

2007-04-10

Permanent link:

<https://doi.org/10.3929/ethz-a-005707448>

Rights / license:

[In Copyright - Non-Commercial Use Permitted](#)

Originally published in:

Journal of Computational Physics 223(1), <https://doi.org/10.1016/j.jcp.2006.09.020>

Higher moments of the velocity distribution function in dense–gas shocks

Stefan Schlamp

*ETH Zurich, Institute of Fluid Dynamics, Sonneggstr. 3, CH–8092 Zürich, Switzerland,
Tel. +41.44.632 5124, Fax +41.44.632 1147*

Bryan C. Hathorn

*Oak Ridge National Laboratories, Division of Computer Science and Mathematics, Oak
Ridge, TN 37831, USA, Tel. +1.865.241 8808, Fax +1.865.574 0680*

Abstract

Large-scale molecular dynamics simulations of a $M_s = 4.3$ shock in dense argon ($\rho = 532 \text{ kg/m}^3$, $T = 300 \text{ K}$) and a $M_s = 3.6$ shock in dense nitrogen ($\rho = 371 \text{ kg/m}^3$, $T = 300 \text{ K}$) have been performed. Results for moments (up to order 10) of the velocity distribution function are shown. The excess even moments of the shock-normal velocity component (i.e., in the direction of shock propagation) are positive for most parts of the shock wave, but become negative towards the hot side of the shock before reverting back to zero. The even excess moments of the shock-parallel velocities and the odd moments of the shock-normal velocity do not change signs within the shock. The magnitude of the excess moments increases with the order of the moment, i.e., the higher moments correspond less and less to those of a Maxwell–Boltzmann distribution.

Key words: shock wave, alignment, orientation, angular momentum, nitrogen, 2-center Lennard–Jones

PACS: 47.40.-x, 31.15.Qg, 31.70.Hq, 47.61.Cb

Email addresses: schlamp@ifd.mavt.ethz.ch (Stefan Schlamp),
hathornb@ornl.gov (Bryan C. Hathorn).

URLs: <http://www.ifd.mavt.ethz.ch/> (Stefan Schlamp),
<http://www.csm.ornl.gov/> (Bryan C. Hathorn).

Nomenclature

a	speed of sound
amu	atomic mass unit
\underline{c}	molecular velocity in α -direction
ϵ_{LJ}	Lennard–Jones well depth
δx	spatial resolution in x -direction
\underline{I}	inertia tensor
k_B	Boltzmann constant
L_α	extent of computational domain in α -direction
Λ	shock thickness
m	mass of molecule
M_s	shock Mach number
$\mu_{i,\alpha\beta\dots}$	i th central moment, $\alpha\beta\dots$ tensor component
N	number of particles in interrogation region
$\underline{\xi}$	location of particle
p	pressure
\tilde{q}	normalized quantity: $(q - q_1)/(q_2 - q_1)$
q_1	pre-shock value
q_2	post-shock value
$rdof$	rotational degrees of freedom
ρ	density
σ_{LJ}	Lennard–Jones radius
u_s	shock speed
\underline{u}_α	macroscopic flow velocity in α -direction
T	temperature
T_α	directional (α -direction) translational temperature
T_{rot}	rotational temperature
x	direction along shock-normal (flow direction)
$\underline{\omega}$	rotation rate vector

1 Introduction

All common macroscopic governing equations of fluid mechanics are derived from the Boltzmann equation. The Euler and the Navier–Stokes equations, for example, are the zeroth and first order series expansions with respect to the Knudsen number (Chapman–Enskog expansion). The closure problem consists of expressing the heat flux and the stress tensor as a function of the other quantities. This implicitly results in making certain assumptions about the moments of the velocity distribution function above some order. The Euler equations, for example, follow from the Boltzmann equation in the high collision rate limit. In this limit, the molecular velocities follow an equilibrium, i.e., Maxwell–Boltzmann distribution, for which all odd moments are zero. The Navier–Stokes equations account for non-zero skewness, but similar assumption for the moments of order four and up are required in their derivation from the Boltzmann equation. Higher-order terms of the Chapman–Enskog series are the Burnett and super–Burnett equations, for which the closure problem is shifted to moments of order 5 and 6, respectively [1].

The errors due to these assumptions are usually small, because the higher moments predominantly affect the tails of the distribution function, i.e., only a small absolute number of molecules. Heat conduction and the viscous stresses, for example, can usually be modeled by the Fourier law and Newtonian behavior. In certain applications, however, a small number of particles with very high kinetic energy can significantly influence the overall behavior of the flow. In chemically reacting flows, for example, few very fast particles are responsible for initiating the reaction chain by creating radicals through high–energy collisions.

Errors are also more significant in the presence of very strong gradients and if the characteristic length scales become comparable to the mean free path (non-zero Knudsen number). This is the case in shock waves, where it has been shown that the Navier–Stokes equations do not yield the correct shock structure for Mach numbers greater than 2 [2]. For dilute gases, the validity of these assumptions can be verified by solving the Boltzmann equation directly e.g. by Direct Boltzmann CFD or Direct Simulation Monte Carlo (DSMC) methods to the desired accuracy. In this limit, the Boltzmann equation is the correct atomistic governing equation.

This is not the case for dense gases and liquids. This is because it only considers uncorrelated binary collisions. At elevated densities, many–particle collisions and correlated collisions become increasingly important [3]. The verification is thus more elaborate.

2 Scope and itinerary

Large-scale Molecular Dynamics (MD) simulations have been performed of a $M_s = 4.28$ shock in dense argon and of a $M_s = 3.56$ shock in dense nitrogen. MD does not require a priori knowledge of or assumptions about the equation of state, transport coefficients, or the velocity distribution function. Its disadvantage is that the computational cost is significantly higher than for DSMC. MD has been applied repeatedly for this fluid mechanical problem (e.g. Refs. 4–6). These works focus on the steady-state profile. They reproduce the overshoot of the translational temperature perpendicular to the plane of the shock wave, which has been predicted by Yen [7]. Holway [8] and Salwen et al. [9] even observe a slight ($\sim 2\%$ for high shock Mach numbers) overshoot of the overall temperature. A setup similar to the one used here, namely the creation of the shock by an impulsively accelerated piston, has been studied by MacPherson [10], Horowitz et al. [11] and Woo & Greber [12]. They obtain temporally resolved data for the formation of the steady state profile from an initially quiescent fluid. All of the above only consider monatomic gases, i.e., do not consider rotational degrees of freedom. Steady-state profiles for a shock in dilute nitrogen has been obtained using a hybrid method (MD + Direct Simulation Monte Carlo) by Tokumaso & Matsumoto [13]. In the present work, for the first time, the shock structure of a diatomic dense fluid has been determined solely by MD.

The results presented in this paper will aid to evaluate the applicability of specific atomistic and macroscopic governing equations to shock wave-type flows in dense fluids. Additionally, we report on a peculiar behavior of the even moments, which we find to have a sign reversal within the shock before relaxing back to zero. This behavior is observed for both fluids. While we cannot extend this result to dilute fluids from our results alone, we do not expect this phenomenon to be an intrinsically dense-gas effect. For dilute fluids, the existence of such a sign reversal could be verified from existing numerical and even experimental velocity distribution functions. Yet, to our knowledge, findings to this effect (if indeed present) have not been reported in the literature. There, the common macroscopic quantities (density, mean velocity, temperature) or raw velocity distribution functions are shown.

The next section will describe the numerical setup and Sec. 4 addresses the data analysis. Sec. 5 will show the behavior of the higher moments across the shock wave and will also briefly describe the overall shock structure. A more detailed discussion of the shock structure and of the shock formation and reflection processes will be reported elsewhere. Sec. 6 examines error and uncertainty issues, to which the higher moments are particularly susceptible, when they are based on a finite sample size. Sec. 7, finally, will summarize the key findings and draw some conclusions from the results.

3 Setup

The molecular dynamics code used is a modified version of *Moldy* [14]. The modifications are to allow moving walls ('frameworks') and non-cubic domains. The computational domain is a cuboid with dimensions $L_x \times L_y \times L_z = 252 \times 237.9 \times 237.9 \text{ \AA}^3$. A layer of 15.86 \AA thickness on either side of the domain (in x -direction) is occupied by a piston and by a stationary wall. Both are modeled by a cubic-face-centered lattice of argon atom such that the number density of the wall structures matches that of the fluid. The details of the wall treatment are not relevant for the purpose of this work, since data is only averaged over times steps where the shock wave is at least 50 \AA from either wall. During this period, the shock moves at a constant speed.

100,000 nitrogen molecules are randomly distributed within the fluid portion of the domain and given random initial velocities and rotation rates drawn from a Maxwell-Boltzmann distribution. The rigid nitrogen molecule is modeled by a two-center Lennard-Jones (6,12) potential with $\sigma_{LJ} = 3.318 \text{ \AA}$, $\epsilon_{LJ}/k_B = 35.6 \text{ K}$, and a bond length of 1.098 \AA between the two Lennard-Jones centers. Each atom has a mass of 14 amu. These parameters correspond to those given by Murthy et al. [15], but the five point-charges are omitted. This is for computationally efficiency reasons and to allow comparisons with alternative approaches for which the incorporations of electrostatic forces is not straight-forward. Vibrations can be neglected in the temperature range considered and the rotational energy levels can be approximated as being continuous. The argon atom is modeled by a Lennard-Jones potential with $\sigma_{LJ} = 3.3952 \text{ \AA}$ and $\epsilon_{LJ}/k_B = 116.79 \text{ K}$ [16]. The mass of the argon atom is 39.948 amu. A cut-off radius for the summation of the short-range forces of 15.6 \AA has been used. Note that this value is significantly larger than the cut-off radius commonly used.

The system is equilibrated during 2 ps, where the molecular velocities and rotation rates are rescaled periodically to correspond to the desired initial temperature of 300 K. This temperature is above the critical temperatures for argon (150.9 K) and nitrogen (126.2 K) such that all states encountered in the simulation are in the supercritical phase. The proper equilibration is verified in a test run with stationary walls. Over the simulation time (12.5 ps), the temperature increase for the argon case was $< 0.1\%$ (N_2 : 0.5%). The time steps are 0.002 ps and 0.0002 ps for argon and nitrogen, respectively. The smaller time step for the nitrogen simulations is due to the requirement that the rotational motion has to be resolved. The shock wave is created by impulsively accelerating the left wall (piston) to a velocity of $u_p = 1,000 \text{ m/s}$. The molecular positions, velocities, orientations (expressed as quaternions), and rotation rates are saved every 0.05 ps. 10 ensembles with perturbed initial conditions are simulated and all data is ensemble averaged.

The argon simulations were performed on single-processor machines. Each time

step of a 100k fluid atoms simulation required 5.5 CPU seconds on a 1.7 GHz AMD Athlon XP processor. Including equilibrations and equilibration verification runs, the ten ensembles hence required approximately 100 CPU hours. The nitrogen cases took approximately 10 CPU seconds per time step on such a single-processor machine. This would result in a total computational cost of 2,000 CPU hours.

Therefore, the nitrogen cases were computed on between 16 and 32 1.3 GHz Power4 processors on a single p690 node of Oak Ridge National Laboratory’s Cheetah facility. Unfortunately, the version of Moldy used does not parallelize very well, because all data is copied to each processor. The time required for the data transfer between processors after each time step then becomes significant compared to the computational cost. While no detailed studies were performed on Cheetah, based on tests on other multi-processor computers, we estimate that the realized speedup was only about 50% of the theoretically achievable speedup. Data analysis also required significant computational resources mainly due to the large amounts of data (> 100 GB), which had to be loaded and processed several times.

4 Data analysis

Steady-state data is temporally averaged by mapping the molecular locations onto a shock-fixed coordinate system. The instantaneous location of the shock wave is obtained by a least-squares fit of a Mott-Smith profile [17] to the density field across the domain. While the density profile is not perfectly described by this functional, this approach does provide a reliable method to locate the shock wave accurately. Temporal averaging is only performed while the shock wave is at least 50 Å from either end wall to rule out end wall effects. 70 (N₂: 69) data sets meet this criterion. Data is analyzed in slices of $\delta x = 0.25$ Å thickness such that each slice contains between approximately 75,000 and 155,000 molecules.

In the shock-fixed frame of reference, flow is from left to right, i.e., the cold side corresponds to $x \rightarrow -\infty$ and the hot side is at $x \rightarrow +\infty$ (the x -direction is reversed from the lab-fixed frame of reference). The origin is chosen such that the nondimensional density $(\rho - \rho_1)/(\rho_2 - \rho_1) = 0.5$ (where the subscripts 1 and 2 correspond to the pre- and post-shock state, respectively) at $x = 0$. We do not nondimensionalize the shock-normal coordinate by the mean-free path, because the concept of the mean-free path is not applicable to dense fluids, where each molecule interacts (collides) continuously with several neighboring molecules.

Let $\underline{\xi}^i = (\xi, \eta, \zeta)$ and \underline{c}^i be the location and the velocity vector of molecule i in the shock-fixed reference frame, respectively. We define the central moments as

follows:

$$\mu_0 = N = \sum_{i=1}^N 1 \quad (1a)$$

$$\mu_{1,\alpha} = \underline{u} = \frac{1}{N} \sum_{i=1}^N \underline{c}_\alpha^i \quad (1b)$$

$$\mu_{2,\alpha\beta} = \sigma_{\alpha\beta}^2 = \frac{1}{N} \sum_{i=1}^N (\underline{c}_\alpha^i - \underline{u}_\alpha(\xi^i)) (\underline{c}_\beta^i - \underline{u}_\beta(\xi^i)) \quad (1c)$$

$$\mu_{3,\alpha\beta\gamma} = \frac{1}{N} \sum_{i=1}^N (\underline{c}_\alpha^i - \underline{u}_\alpha(\xi^i)) (\underline{c}_\beta^i - \underline{u}_\beta(\xi^i)) (\underline{c}_\gamma^i - \underline{u}_\gamma(\xi^i)) \quad (1d)$$

⋮

Greek subscripts denote spatial components of vectors or tensors. Roman subscripts indicate the order of the moment. All tensor components are computed up to μ_3 . For μ_k ($k \geq 4$) only the diagonal elements ($\alpha = \beta = \gamma = \dots$) are calculated. The sum is over all molecules within a slice $|x - \xi^i| \leq \delta x/2$. Note that the finite spatial resolution would lead to a bias in the presence of velocity gradients, i.e., if \underline{u} changes across a slice. To minimize this bias, \underline{u} is linearly interpolated to each molecule's location when calculating the third and higher moments.

The translational directional temperatures are related to the second moment by

$$T_\alpha = \frac{m\mu_{2,\alpha\alpha}}{3k_B} \quad (2)$$

The translational temperature is $T_{trans} = T_x + T_y + T_z$ and the overall temperature is $T = (3T_{trans} + rdof \times T_{rot}) / (3 + rdof)$, where $rdof$ is the number of rotational degrees of freedom of the molecule and where T_{rot} denotes the rotational temperature,

$$T_{rot} = \frac{1}{3Nk_B} \sum_{i=1}^N \underline{\omega}^{iT} \underline{I} \underline{\omega}^i. \quad (3)$$

\underline{I} and $\underline{\omega}$ are the moment of inertia tensor and the rotation rate vector, respectively.

The third and higher moments are normalized by the respective power of the standard deviation $\sigma_{\alpha\alpha}$. Just as the temperature can be related to the second moment, the heat flux vector can be related to the third central moment. The fourth and higher even moments are expressed as excess moments, i.e., the value of the moment which a Maxwell–Boltzmann distribution would have is subtracted ($\mu_{4,MB} = 3$, $\mu_{6,MB} = 15$, $\mu_{8,MB} = 105$, $\mu_{10,MB} = 945$). An equilibrium distribution would thus correspond to an excess moments of zero.

5 Results

Table 1 summarizes the property changes across the shock waves. The pre-shock densities correspond to the same number density of $n = 8.02 \times 10^{27} \text{ m}^{-3}$. The pre-shock density for argon corresponds to its liquid-vapor critical point density. The pre-shock temperature, however, is approximately twice the critical temperature such that near-critical effects are not present. The temperature range for nitrogen is such that the rotational energy levels can be assumed continuous ($T_1 \gg \Theta_r = 2.88 \text{ K}$ [18]) and vibrations can be neglected ($T_2 \ll \Theta_v = 3,374 \text{ K}$ [18]). The assumptions of classical mechanics regarding the rotational excitation and of rigid molecules are thus justified. The flow velocities given in Table 1 are in the lab-fixed frame of reference to show that the post-shock velocities deviate slightly from the piston speed. This is due to fluid molecules leaking into the piston. The leak rate is lower for nitrogen because of the larger size of the nitrogen molecule and because of the lower post-shock temperature than for the argon case. The pressure is included for indicative purposes only. The pressure and the speed of sound do not follow directly from our MD results, but are calculated from reference-type empirical equations of state suggested by the National Institute of Standards and Technology (NIST). Upstream and downstream of the shock, the fluid is in equilibrium such that the macroscopic equations of state are applicable. Note that these semi-empirical equations of state do not enter the simulation in any way. They are only used to calculate the shock Mach number and the pressures for indicative purposes. In particular our nitrogen model might result in deviations from the behavior of real nitrogen. Table 1 also gives a characteristic length scale closely related to the mean-free path in dilute gases.

Fig. 1 shows the variation of the density (μ_0) and the temperature components (μ_2) across the shock wave. The mean flow velocity (μ_1) is not shown for clarity. It closely follows the line for T_y . If desired, the velocity profile can be calculated from the density profile and the continuity equation. The quantities shown undergo a net change across the shock wave. It is thus convenient to nondimensionalize them by their pre- and post-shock quantities, $\tilde{q} = (q - q_1)/(q_2 - q_1)$. T_x shows the familiar overshoot in the shock wave. Its peak magnitude is 23.96% and 44.3% for argon and nitrogen, respectively. It is due to the finite coupling rates between the translational degrees of freedom (and also due to finite-rate translational-rotational mode coupling in the case of nitrogen). The overshoot for the argon case is surprisingly close to the value predicted for a shock of the same Mach number in a dilute fluid (23.6%) [7]. There is no observable overshoot of the overall temperature.

The shock-normal temperature change leads all other quantities. For argon, the temperature changes upstream of the velocity, followed by a change of the density. This means that higher moments change upstream of lower moments. This can be understood by considering that a small number of fast molecules entering the shock wave are sufficient to change the higher moments, but they are negligible for the

Table 1

Pre- and post shock conditions of the simulated shock waves in argon and nitrogen. The shock Mach numbers are based on a tabulated speeds of sound.

			Argon		Nitrogen	
		unit	pre-shock	post-shock	pre-shock	post-shock
density	ρ	kg/m ³	532.1	1,086.7	370.9	741.0
nondim. density	$\rho/(n\sigma_{LJ}^3)$	–	3.19	1.57	3.42	1.71
number density	n	10 ²⁷ m ⁻³	8.0	16.3	8.0	16.0
mean molecular spacing	$n^{-1/3}$	Å	5.0	3.94	5.0	3.97
”mean-free path” [§]	$1/(n\sigma_{LJ}^2)$	Å	10.8	5.3	11.4	5.7
temperature	T	K	301.0	1,757.1	300.1	978.0
nondim. temperature	$T/(k_B\epsilon_{LJ})$	–	2.57	15.0	8.43	27.5
velocity	u	m/s	0	967.2	0	985.1
sound speed	a	m/s	440.7*	?	556.7 [†]	1722.4 [†]
pressure	p	MPa	34.12*	?	42.3 [†]	689.5 [†]
shock speed	u_s	m/s		1,885.0		1,976
shock Mach number	M_s	-		4.28		3.56
shock thickness [‡]	Λ	Å		8.85		7.51

[†] Calculated from equation of state of Span et al. [19]

* Calculated from equation of state of Tegeler et al. [20] The post-shock state is out of the range of validity of the equation of state.

[‡] Based on the maximum density gradient, $\Lambda = (\rho_2 - \rho_1)/(\partial\rho/\partial x)_{max}$.

[§] This characteristic length scale is related to the mean-free path and is given here for indicative purposes only.

mean and their number is small compared to the absolute number of particles. It will be shown later that this trend does not continue indefinitely for the moments of order 4 and higher. The location where these moments start to change approaches a limit.

For nitrogen, the presence of rotational degrees of freedom changes the behavior. While the temperature profile initially lies upstream of the velocity profile, the order is reversed for $x \geq 2$ Å. This is because the energy transfer between the translational degrees of freedom is faster than between the translational and rotational degrees of freedom. Note how the rotational temperature lags even the density profile on the hot side of the shock wave.

The shock structures shown in Fig. 1 resemble qualitatively those for shocks in dilute gases. There are some significant differences, however. The shock thickness relative to the mean-free path is thicker in dense fluids for a shock of the same

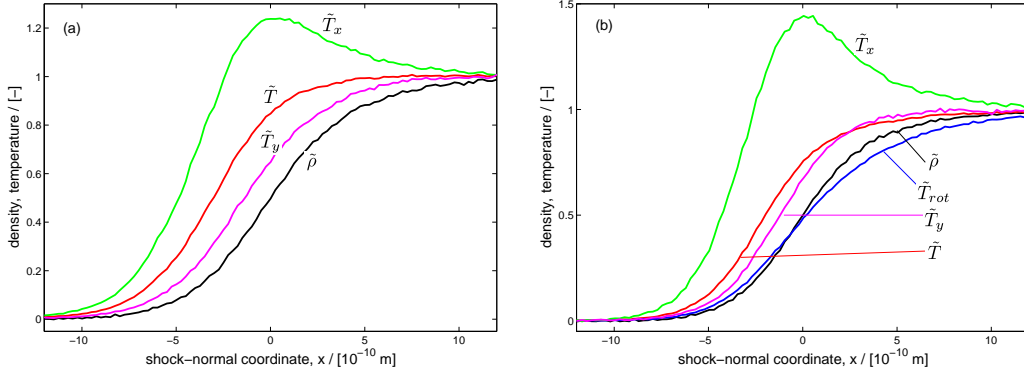


Fig. 1. Shock structure in argon (a, left) and nitrogen (b, right). The velocity profile (not shown for clarity) is similar to T_y .

Mach number. We also observe deviations of the shape of the density profile. The asymmetry parameter as defined by Schmidt [21] is greater than unity in dilute gases at comparable Mach numbers, but it is 0.8 and 0.72 for the argon and nitrogen cases considered here, respectively

Fig. 2 shows the higher central moments of the velocity distribution function across the shock wave for the argon (a) & (b) and the nitrogen (c) & (d) case. The even moments are plotted in Fig. 2(a) & (c), the odd moments in Fig. 2(b) & (d). Because the behavior is qualitatively the same for both fluids, we will base the following discussion on the nitrogen case. A discussion about the differences and noteworthy commonalities between the argon and the nitrogen shock waves will follow.

Fig. 2(c) shows the excess moments for the nitrogen shock. The solid lines are for the direction along the direction of the main flow. The dotted lines are for one of the in-plane velocity components. Upstream and downstream, all excess moments are zero, consistent with a Maxwell–Boltzmann distribution of a fluid in equilibrium. The shock–normal moments of all orders simultaneously start to deviate from zero at $x \approx -12 \text{ \AA}$. This location coincides with the location where the first increase of T_x (Fig. 1(b)) can be observed. The excess kurtosis has a peak at $x \approx -5 \text{ \AA}$. This is upstream of where the peak temperature overshoot is observed ($x \approx 0 \text{ \AA}$). The location of the peak moves upstream with increasing order of the moment. The data for $\mu_{8,x}$ and $\mu_{10,x}$ exhibits large fluctuations, which are strongly correlated within a region on the cold side of the shock. The peak excess moments increase with the order of the moment. Note the scaling, which has been applied to the plotted data in Fig. 2. Positive excess central moments represent distributions which have fat tails compared to the Maxwell–Boltzmann distribution.

The excess kurtosis in the shock normal direction ($\mu_{4,x}$) becomes negative at $x \approx -1.5 \text{ \AA}$ and approaches zero very slowly thereafter. $\mu_{6,x}$ and $\mu_{8,x}$ also become negative, but to a lesser degree than $\mu_{4,x}$ – relative to the positive peak value. $\mu_{10,x}$ might also become negative, but not significantly above the uncertainty.

The shock–parallel even moments are always non–negative. They start deviating from zero further downstream ($x \approx -8 \text{ \AA}$) and their peak amplitude is lower than for the shock–normal direction. They also show the trend that the peak shifts upstream with increasing order of the moment. The ratio $\max(\mu_{i,x})/\max(\mu_{i,y})$ decreases with increasing i , i.e., the deviations from a Maxwell–Boltzmann distribution become less important for the shock–parallel velocities compared to the deviations for the shock–normal velocities.

The odd moments are shown in Fig. 2(d). They are negative indicating that the velocity distribution function leans towards less positive velocities. The flux of translational kinetic energy is proportional to $\mu_{3,x}$. $\mu_{3,x} < 0$ corresponds to a heat flux from the hot side of the shock wave towards the cold side, i.e., against the flow direction. As for the even moments, the peaks shift upstream with increasing order. The magnitudes also increase with increasing order, but the increase is slower than for the even moments. The scaling factors in Figs. 2(c) & (d) are the same for a given order. Note the different relative amplitudes $\mu_{4,x}/\mu_{6,x}$ vs. $\mu_{3,x}/\mu_{5,x}$.

The off–diagonal elements of μ_2 and μ_3 are not shown. They exhibit the expected result, which can be summarized as follows: $\mu_{2,\alpha\beta} = 0$ for $\alpha \neq \beta$, i.e., the different components of the velocity vector are not correlated. This has the convenient result that the velocity distribution function with respect to cylindrical velocity components $f(c_x, (c_y^2 + c_z^2)^{1/2})$ contains the same information as the three–dimensional (in phase–space) distribution function $f(c_x, c_y, c_z)$.

The only non–zero off–diagonal elements of μ_3 are $\mu_{3,x\alpha\alpha}$ for any α . These terms are related to the flux of kinetic energy stored in the molecular velocity fluctuations along the α –direction in the x –direction. Since there cannot be a heat flux in the shock–parallel directions and because the different components of the velocity vector are not correlated, the other components must be zero.

The behavior for the argon shock wave is qualitatively similar and we next discuss the differences between the two cases. Note that the Mach number is not the same for both cases such that the comparison should not be over–interpreted. For both shocks, the initial number density and $\Delta u = u_2 - u_1$ are the same. Also note in Table 1 that the shock speeds are very similar. Likewise, the molecular sizes ($\sigma_{LJ,Ar} \sim \sigma_{LJ,N_2}$) are comparable and the larger collision cross section of the nitrogen molecule is largely due to the bond length. The different shock Mach numbers can thus be traced back to the different sound speeds in the pre–shock fluid state, which itself can largely be explained by the difference in the molecular weight. Despite the different Mach numbers, the density ratio across both shocks is approximately 2 (Ar: 2.04; N₂: 2.00). The temperature ratio (Ar: 5.84; N₂: 3.26) shows the largest discrepancy of the macroscopic quantities. But the same trend is observed for shocks in perfect gases: for a given shock Mach number, the temperature ratio increases with the ratio of specific heats, i.e., is higher for monatomic fluids than for polyatomic fluids. It is due to the additional degrees of freedom available for en-

ergy deposition. The temperature is proportional to the average energy *per degree of freedom* such that the overall temperature ratio is thus reduced in the presence of rotational degrees of freedom.

The differences between Fig. 1(a) and Fig. 1(b) have been addressed above. We thus now turn to the differences exhibited between Figs. 2(a) & (c) and Figs. 2(b) & (d). First note the different absolute magnitudes of the moments. The peak excess kurtosis for argon is approximately three times higher than that for nitrogen. This discrepancy cannot be explained by the different temperature levels, because all moments are normalized by the temperature ($T \sim \mu_2$). The trend is exaggerated for the higher moments. The scaling factors in Fig. 2 for both fluids are the same. While the curves for the even moments in Fig. 2(a) have similar (scaled) amplitudes, this is not the case in Fig. 2(c). For nitrogen, the magnitude of the higher moments relative to lower-order moments is lower than for argon. The same trend is observed for the odd moments, but here the absolute magnitude of the skewness in shock-normal direction is very similar.

Also note the blips around $x = -15 \text{ \AA}$ and $x = -10 \text{ \AA}$ in Figs. 2(a) & (c), respectively. Additional numerical experiments would have to confirm if these are physical or noise. A corresponding blip is observed in Fig. 2(b). One could interpret these as evidence of the first collisions of molecules entering the shock; they would correspond to unusually slow molecules. Yet it is curious why the moments would plateau on a low level for several angstroms before suddenly increasing in magnitude.

The strong fluctuations of the higher moments are restricted to the cold side of the shock waves. We hypothesize that the fluctuations are due to the few remaining fast molecules, which have entered the shock from the left and have not been slowed down through interactions. On the cold side of the shock, no uninhibited molecules have remained.

Two-dimensional (in phase space) velocity distribution functions, $f(c_x, (c_y^2 + c_z^2)^{1/2})$ have also been evaluated, but the sample sizes were not sufficient to analyze them with respect to higher statistical moments. Yet they allow one to calculate the collision operators and to compare them with different approximations. These will be presented in the context of a detailed discussion of the shock structure.

6 Discussion

Previous DSMC simulations for dilute gases at moderate Mach numbers [22] and for infinite-Mach number shocks in a dense hard-sphere fluid [23] have produced overshoots of the overall temperature within the shock wave. Neither for argon nor for nitrogen has an overshoot of the temperature been observed, which was

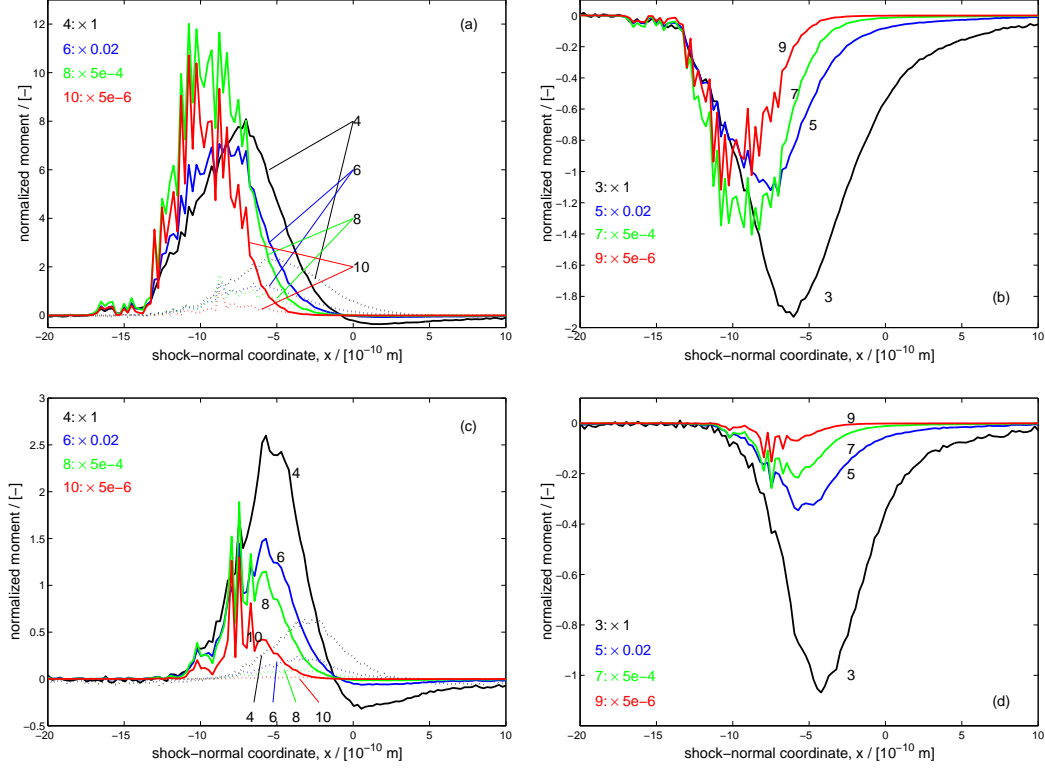


Fig. 2. Moments of the velocity distribution function for a shock wave in dense argon (a, top left) & (b, top right) and nitrogen (c, lower left) & (d, lower right). The labels indicate the order of the moment. The solid lines are for the molecular velocities in shock-normal direction, the dotted lines for velocities within the shock plane. The odd moments for the shock-parallel velocities are zero (within the measurement uncertainty) and are not shown. The curves are scaled to fit in the same axes. The scaling factors, which have been applied for each order, are shown in each panel.

clearly discernible from the noise in the data, whereas Ohr [22] and Cercignani et al. [23] observe overshoots of several percent. The results presented here put an upper bound of $< 0.5\%$ on any possible temperature overshoot.

As pointed out in Sec. 4, the average velocity is linearly interpolated to each molecule's position when calculating the moments. We also used higher-order interpolation schemes and used different spatial resolutions. Neither of which changed the results shown in Sec. 5 significantly.

By calculating the higher moments based on a finite number of realizations from a probability density function, errors are introduced. The average value of the moments in the pre- and post-shock regions, which are unaffected by the shock wave, corresponds to the value of a Maxwell-Boltzmann distribution within the uncertainty (Table 2). For the even moments, the average deviation is approximately 5% from the Maxwell-Boltzmann value (averaging over the same regions as in Table 2). For the odd moments, the deviations lie between those of the two neigh-

Table 2

Estimates of the statistical noise in the data in the pre-shock and the post-shock state. Standard deviation of the excess moments over 20 slices upstream ($-25 \text{ \AA} \leq x \leq 20 \text{ \AA}$) and downstream ($20 \text{ \AA} \leq x \leq 25 \text{ \AA}$) of the shock wave. Percentage values can be only given for quantities, which are not zero for a fluid in equilibrium.

quantity	unit	Argon		Nitrogen	
		pre-shock	post-shock	pre-shock	post-shock
ρ	[kg/m ³]	1.60 (0.30%)	2.35 (0.22%)	1.25 (0.34%)	1.45 (0.20%)
u	[m/s]	0.71 (0.04%)	1.78 (0.19%)	0.93 (0.05%)	2.11 (0.21%)
T	[K]	0.45 (0.15%)	1.42 (0.08%)	0.26 (0.09%)	1.20 (0.12%)
$\frac{\mu_3}{\sigma^3}$	[-]	0.01	0.01	0.01	0.01
$\frac{\mu_4}{\sigma^4} - 3$	[-]	0.04	0.04	0.03	0.04
$\frac{\mu_5}{\sigma^5}$	[-]	0.09	0.10	0.09	0.09
$\frac{\mu_6}{\sigma^6} - 15$	[-]	0.41	0.38	0.29	0.40
$\frac{\mu_7}{\sigma^7}$	[-]	0.94	1.22	1.18	0.99
$\frac{\mu_8}{\sigma^8} - 105$	[-]	5.34	4.34	3.90	4.84
$\frac{\mu_9}{\sigma^9}$	[-]	13.8	18.6	20.6	15.6
$\frac{\mu_{10}}{\sigma^{10}} - 945$	[-]	81.3	64.8	87.9	70.5

boring even moments. Table 2 gives estimates for the uncertainty. It shows the fluctuations of the moments in the pre- and post-shock regions, i.e., the standard deviation of the moments. Because of the very similar number densities for both cases in both regions, one expects comparably similar uncertainties. Table 2 shows that this is the case.

The odd moments of the in-plane velocities were not plotted in Fig. 2. With the scaling applied there, i.e., relative to the respective moment in the shock-normal direction, they are close to zero. In absolute terms, however, they fluctuate around zero much stronger than the values in Table 2 would suggest. Their magnitude is typically only one order of magnitude smaller than the same moment for the shock-normal velocities. There cannot be a macroscopic flow or heat flux in the in-plane directions since there is no preferred direction. This does not apply at every instance in time and on a microscopic level. The fluctuations of the odd moments around zero within the shock wave are not unphysical on the length and time scales considered, but they would average out to zero for larger sample sizes.

Also, the large correlation between the higher moments (μ_8 and μ_{10}) have to be noted. These are due to the fact that a decreasing number of molecules in the tails of the distribution function have an increasing impact on the higher moments. This hence constitutes another finite sample size effect.

7 Conclusions

It was shown that the even moments of order four and higher of the velocity distribution function across a shock wave exhibit a sign reversal. They are positive on the cold side of the shock, but slightly negative on the hot side of the shock. This means that the velocity distribution function changes from having fat tails to having slim tails, at least with respect to the molecular velocities along the shock-normal direction. The distribution function for the in-plane velocity components does not have a sign reversal. We do not expect that this is a dense gas effect. Experimental [24–26] and numerical [27–35] data for dilute gases, from which the higher moments can be extracted, is available in the literature, but to the authors’ knowledge, the effect has not been reported previously. The location where the higher out-of plane moments first deviate from zero does not depend on the order of the moment, i.e., the trend for the lower moments that the temperature (second moment) changes upstream of the flow velocity (first moment) and the density (zeroth moment) is not continued or it approaches a limit asymptotically. We also observe, that the odd moments of the in-plane velocity distribution function fluctuate strongly around zero within the shock wave.

The magnitude of the higher moments does not decrease with the order of the moment. The opposite is observed. This is significant when considering appropriate closure relations for the atomistic governing equations when deriving macroscopic governing equations from them. The influence on the macroscopic quantities will, for most practical purposes, be negligible because the higher moments are predominantly affected by the (few) particles in the tails of the distribution function. The effect could, however, be large for flows in which high kinetic energy collisions play a significant role, such as for chemically reacting flows.

Acknowledgments

This work was sponsored by the Division of Computer Science and Mathematics and used resources of the Center for Computational Sciences at Oak Ridge National Laboratory, which is supported by the Office of Science of the U.S. Department of Energy under Contract No. DE-AC05-00OR22725.

References

- [1] C. Cercignani, *The Boltzmann Equation and its Applications*, Springer-Verlag, New York, 1988.

- [2] J. P. Elliott, Validity of Navier–Stokes relation in a shock–wave, *Canadian Journal of Physics* 53 (6) (1975) 583–586.
- [3] E. G. D. Cohen, Fifty years of kinetic theory, *Physica A* 194 (1–4) (1993) 229–257.
- [4] B. L. Holian, W. G. Hoover, B. Moran, G. K. Straub, Shock–wave structure via non–equilibrium molecular–dynamics and Navier–Stokes continuum mechanics, *Physical Review A* 22 (6) (1980) 2798–2808.
- [5] E. Salomons, M. Mareschal, Usefulness of the Burnett description of strong shock waves, *Physical Review Letters* 69 (2) (1992) 269–272.
- [6] O. Kum, W. G. Hoover, C. G. Hoover, Temperature maxima in stable two–dimensional shock waves, *Physical Review E* 56 (1) (1997) 462–465.
- [7] S. M. Yen, Temperature overshoot in shock waves, *Physics of Fluids* 9 (7) (1966) 1417–1418.
- [8] L. H. Holway, Temperature overshoots in shock waves, *Physics of Fluids* 8 (10) (1965) 1905–1906.
- [9] H. Salwen, C. E. Grosch, S. Ziering, Extension of the Mott–Smith method for a one–dimensional shock wave, *Physics of Fluids* 7 (2) (1964) 180–189.
- [10] A. K. Macpherson, Formation of shock waves in a dense gas using a molecular–dynamics type technique, *Journal of Fluid Mechanics* 45 (1971) 601–621.
- [11] J. Horowitz, M. Woo, I. Greber, Molecular dynamics simulation of a piston–driven shock wave, *Physics of Fluids (Gallery of Fluid Motion)* 7 (9) (1995) S6.
- [12] M. Woo, I. Greber, Molecular dynamics simulation of piston-driven shock wave in hard sphere gas, *AIAA Journal* 37 (2) (1999) 215–221.
- [13] T. Tokumasu, Y. Matsumoto, Dynamic molecular collision (DMC) model for rarefied gas flow simulations by the DSMC method, *Physics of Fluids* 11 (7) (1999) 1907–1920.
- [14] K. Refson, Moldy: A portable molecular dynamics simulation program for serial and parallel computers, *Computer Physics Communications* 126 (3) (2000) 310–329.
- [15] C. S. Murthy, S. F. O’Shea, I. R. McDonald, Electrostatic interactions in molecular crystals – lattices dynamics of solid nitrogen and carbon dioxide, *Molecular Physics* 50 (3) (1983) 531–541.
- [16] J. Vrabec, J. Stoll, H. Hasse, A set of molecular models for symmetric quadrupolar fluids, *Journal of Physical Chemistry B* 105 (48) (2001) 12126–12133.
- [17] H. M. Mott-Smith, The solution of the Boltzmann equation for a shock wave, *Physical Reviews* 82 (11) (1951) 885–892.
- [18] D. A. McQuarrie, *Statistical Mechanics*, HarperCollinsPublishers, New York, 1976.

- [19] R. Span, E. W. Lemmon, R. T. Jacobsen, W. Wagner, A. Yokozeki, A reference equation of state for the thermodynamic properties of nitrogen for temperatures from 63.151 to 1000 K and pressures to 2200 MPa, *Journal of Physical and Chemical Reference Data* 29 (6) (2000) 1361–1433.
- [20] C. Tegeler, R. Span, W. Wagner, A new equation of state for argon covering the fluid region for temperatures from the melting line to 700 K at pressures up to 1000 MPa, *Journal of Physical and Chemical Reference Data* 28 (3) (1999) 779–850.
- [21] B. Schmidt, Electron beam density measurements in shock waves in argon, *Journal of Fluid Mechanics* 39 (1969) 361–373.
- [22] Y. G. Ohr, Improvement of the Grad 13 moment method for strong shock waves, *Physics of Fluids* 13 (7) (2001) 2105–2114.
- [23] C. Cercignani, A. Frezzotti, P. Grosfils, The structure of an infinitely strong shock wave, *Physics of Fluids* 11 (9) (1999) 2757–2764.
- [24] E. P. Muntz, L. N. Harnett, Molecular velocity distribution function measurements in a normal shock wave, *Physics of Fluids* 12 (10) (1969) 2027–2035.
- [25] F. Robben, L. Talbot, Measurement of rotational distribution function of nitrogen in a shock wave, *Physics of Fluids* 9 (4) (1966) 653–662.
- [26] T. Holtz, E. P. Muntz, Molecular velocity distribution–functions in an argon normal shock–wave at Mach–7, *Physics of Fluids* 26 (9) (1983) 2425–2436.
- [27] G. A. Bird, The velocity distribution function within a shock wave, *Journal of Fluid Mechanics* 30 (1967) 479–487.
- [28] M. Perlmutter, Model sampling applied to the normal shock problem, in: *Rarefied Gas Dynamics, Vol. I*, Academic Press, New York, 1969, pp. 327–330.
- [29] G. A. Bird, Aspects of structure of strong shock waves, *Physics of Fluids* 13 (5) (1970) 1172–1177.
- [30] S. M. Yen, W. Ng, Shock–wave structure and intermolecular collision laws, *Journal of Fluid Mechanics* 65 (1974) 127–144 (+ 2 plates).
- [31] S. M. Yen, Numerical solution of the nonlinear Boltzmann equation for nonequilibrium gas flow problems, *Annual Review of Fluid Mechanics* 16 (1984) 67–97.
- [32] G. A. Bird, Perception of numerical methods in rarefied gas dynamics, in: *Rarefied Gas Dynamics: Theoretical and Computational Techniques*, AIAA, Washington, 1989, pp. 211–226.
- [33] D. A. Erwin, G. C. Pham-Van-Diep, E. P. Muntz, Nonequilibrium gas–flows – 1. A detailed validation of Monte–Carlo direct simulation for monatomic gases, *Physics of Fluids A – Fluid Dynamics* 3 (4) (1991) 697–705.
- [34] E. P. Muntz, D. A. Erwin, G. C. Pham-Van-Diep, A review of the kinetic detail required for accurate predictions of normal shock waves, in: *Rarefied Gas Dynamics*, VCH, Weinheim, 1991, pp. 198–206.

[35] G. A. Bird, *Molecular Gas Dynamics and the Direct Simulation of Gas Flows*, Oxford Engineering Science Series; 42, Clarendon Press, Oxford, 1994.